Multifrequency Radar Observations Collected in Southern France during HyMeX-SOP1

Olivier Bousquet, A. Berne, Julien Delanoë, Y. Dufournet, J.J. Gourley, Joël van Baelen, C. Augros, Lucas Besson, B. Boudevillain, Olivier Caumont, et al.

MULTIPLE-FREQUENCY RADAR OBSERVATIONS COLLECTED IN SOUTHERN FRANCE DURING THE FIELD PHASE OF THE HYDROMETEOROLOGICAL CYCLE IN THE MEDITERRANEAN EXPERIMENT (HYMEX)

Capsule: An ambitious radar deployment to collect high quality observations of heavy precipitation systems developing over and in the vicinity of a coastal mountain chain

Submitted to the

Bulletin of the American Meteorological Society

Revised version, February 2014

O. Bousquet [(1)] * , A. Berne [(2)], J. Delanoe [(3)], Y. Dufournet [(4)], J.J. Gourley [(5)], J. Van-Baelen [(6)], C. Augros [(7)], L. Besson [(3)], B. Boudevillain [(8)], O. Caumont [(7)], E. Defer [(9)], J. Grazioli [(2)], D. J. Jorgensen [(5)], P.-E. Kirstetter [(5)], J-F.Ribaud [(7)], J. Beck [(7)] , G. Delrieu [(8)], V. Ducrocq [(7)], D. Scipion [(10)], A.Schwarzenboeck [(6)] and J. Zwiebel [(6)]

(1) LACy, UMR 8105, Météo-France / CNRS / Université de La Réunion, Saint-Denis, France
(2) EPFL / LTE, Lausanne, Switzerland
(3) LATMOS, UMR 8190 UVSQ / ISPL / CNRS, Guyancourt, France
(4) TU Delft, The Netherlands
(5) NOAA/NSSL, Norman, USA
(6) LaMP, UMR6016, CNRS / Université Blaise Pascal, Clermont Ferrand, France
(7) CNRM-GAME, UMR 3589, Météo-France / CNRS, Toulouse, France
(8) LTHE, UMR 5564, CNRS / IRD / Université de Grenoble, Grenoble, France
(9) LERMA, Paris, France
(10) Radio Observatorio de Jicamarca, InstitutoGeofísicodelPerú, Lima, Perú

* CorrespondingAuthor: Olivier Bousquet, Laboratoire de L'Atmosphère et des Cyclones (LACy), St Denis de La Réunion, France. E-mail: olivier.bousquet@meteo.fr

Abstract

The radar network deployed in Southern France during the first Special Observing Period (SOP1) of the Hydrometeorological Cycle in the Mediterranean Experiment (HyMeX) was designed to precisely document the 3-D structure of moist upstream flow impinging on complex terrain as a function of time, height and along-barrier distance as well as surface rainfall patterns associated with orographic precipitation events. This deployment represents one of the most ambitious field experiments yet endeavoring to collect high quality observations of thunderstorms and precipitation systems developing over and in the vicinity of a major mountain chain.

Radar observations collected during HyMeX represent a valuable, and potentially unique, dataset that will be used to improve our knowledge of physical processes at play within coastal orographic heavy precipitating systems as well as to develop, and evaluate, novel radar-based products for research and operational activities. This article provides a concise description of this radar network and discusses innovative research ideas based upon preliminary analyses of radar observations collected during this field project with emphasis on the synergetic use of dual-polarimetric radar measurements collected at multiple frequencies.

Article

The accurate prediction of orographic convective precipitation is a major meteorological challenge that depends on a wide range of time and space scales as well as complex processes ranging from moist orographic airflow dynamics to cloud microphysics. Forecasting the location and amount of heavy precipitation is particularly critical in coastal mountainous regions. Heavy precipitation can indeed generate rapid and destructive floods and thus represent a major threat to lives and infrastructure, especially since communities living in foothill regions have experienced large population increases. Several important field and research programs such as the Mesoscale Alpine Programme (MAP, Bougeault et al. 2001), the Intermountain Precipitation Experiment (IPEX; Schultz et al., 2002) and the Improvement of Microphysical Parameterization through Observational Verification Experiment (IMPROVE, Stoelinga et al. 2003), among others, have been designed in the last decade to improve theunderstanding and prediction of orographically generated precipitation. Although the analysis of datasets collected during these field campaigns has dramatically advanced our understanding of moist dynamics and microphysics over complex terrain (e.g., Medina et al., 2005; Rotunno and Houze, 2007), our knowledge of coastal orographic precipitation remains insufficient to satisfy societal demands for precise forecasts and warnings.

A fundamental element that has been missing in past field experiments is nearly simultaneous measurements of the moist marine inflow as a function of time, height and along-barrier distance with measurements of precipitation over orography in addition to turbulence/microphysical transformations occurring in between. The Hydrometeorological Cycle in the Mediterranean Experiment (HyMeX) field campaign (Ducrocq et al. 2014), which is dedicated to the study of

the water cycle in the northwestern Mediterranean basin, intends to achieve this goal and to gather such basic, but hard-to-obtain, information.

High-resolution dual-Doppler and dual-polarization radar measurements is key to resolving small-scale precipitation and flow structures as well as to study the role of complex topography and microphysical processes in precipitation formation and enhancement. During the first Special Observing Period (SOP1, Fall 2012) of HyMeX, which principally focused on investigating the influence of mountain topography on moist dynamics and cloud microphysics, important efforts have thus been made to achieve comprehensive weather radar coverage. In southern France, the HyMeX radar network was specifically designed to collect high quality observations of thunderstorms and precipitation systems developing over and in the vicinity of the Massif Central mountain chainto documentthe characteristics of the hydrometeors forming within the moist upstream flow impinging on the Cevennes area.

Observations collected in this framework will provide for the investigation of the microphysics and dynamics of mesoscale convectivesystems (MCSs)developing in this flood prone area, and will be used to develop and evaluate innovative radar-based products for numerical weather prediction (NWP) and hydrological applications. A description of this observing network is given hereafter together with a discussion of potential research studies inferred from thepreliminary analysis of radar data collected during HyMeX SOP1.

The HyMeX Experimental Radar network in Southern France

Theprecipitation observingnetwork deployed in Southern France during HyMeX (Fig. 1) consists of a combination of disdrometers and weather radars operating at S, C, X, Ku and W

band (a detailed description of these instruments is available in electronic supplement #1). All these sensors were deployed within, a 90,000 km² domain encompassing the Rhone Valley and extending northwards from the Mediterranean Sea to the Massif Central Mountains and eastwards from the Massif Central to the French Alps.

The core of the radar network is based on a subsample of the French operational radar network ARAMIS (Fig. 1a). It comprises eight radars operating at C- and S-band, which cover the French coastal Mediterranean region with an average radar baseline of 150 km, and two X-band polarimetric radars deployed in the Southern Alps under the auspices of the RHYTMME project (Beck and Bousquet, 2013). During the experimental phase, additional dual-Doppler and dual-polarization radar coverage was also required to more explicitly resolve small-scale microphysical and dynamical processesin complex terrain as well as to collect high-resolution data in areas not well covered by the operational radars. Four transportable X-band scanning weather radars were thus deployed at various locations of the Cevennes-Vivarais area (Fig. 1b) to obtain hydrometeor type, reflectivity, and Doppler velocity measurements in both volume and Range-Height Indicator (RHI) scanning mode.

The NOXP polarimetric Doppler radar, operated by the US National Severe Storm Laboratory (NSSL), was deployed near the foothills of the Massif Central on thetop of Mt. Bouquet (600m amsl). This site, located at an equal distance (~40 km) between the Bollène and Nîmes operational S-band radars, was chosen to allow for high-resolution multiple Doppler analysis of radar data over an area that is particularly prone to extreme flash floods (Delrieu et al. 2005).

Asecond polarimetric radar, MXPOL, was deployed farther north in the vicinity of a high-resolution Hpiconet network (a dense network of raingauges and disdrometers over a watershed

indicated by the red rectangle in Fig. 1b). This radar, operated by Ecole Polytechnique de Lausanne (EPFL, Switzerland), focused on obtaining microphysical characteristics of clouds and precipitation in terms of drop size and shape distribution with an emphasis on shallow orographic rain bands that develop over the Cévennes mountains.

Two fast scanning "conventional" radars (X1 and X2) operated by the French Laboratoire de Météorologie Physique (LaMP) were also deployed in the northern part of the domain to study the variability of rain at the precipitation cell scaleand at high temporal resolution (< 1min). These radars were positioned at La Bombine, a site located on the Cévennes ridge at about 1000m AMSL and approximately 10 km away from the observed maximum climatological rainfall, and at Le Chade, within the Hpiconet area, respectively.

The radar network was completed by radars profilers deployed throughout the area to investigate space-time variability of precipitation as a function of along-barrier distance. These include an ensemble of six Micro Rain Radars (MRR, Löffler-Mang et al. 1999) extending from the Mediterranean coast to the Massif Central Mountains, to collect high-resolution microphysical and kinematic measurements along a coarse cross-barrier transect on the windward slope (southeastern foothills of the Massif Central), and the S-band,dual-polarimetric, radar profiler TARA (Unal, 2009; Dufournet et al 2011), operated by the Delft University of Technology.

Finally, a network of disdrometers composed of 27 "Parsivel" (Loffler-Mang and Joss, 2000) and two two-dimensional video-disdrometers (2DVD, Kruger and Krajewski 2002) was also installed to complement the already dense surface observation network available over the area (Delrieu 2003). The 2DVD provides information about the shape of hydrometeors through

recording two orthogonal side views of every particles falling through a 10x10 cm² sampling area. The Parsivel is an optical disdrometer with a sampling area of ~50 cm² that is commonly used to investigate the micro-structure of rainfall. About half of the disdrometers were concentrated in the northern part of the experimental domain, within the ~35 km² Hpiconet area. The remaining ones were deployed at various locations along the MRR transect.

This experimental setup was also complemented by the 95 GHz airborne cloud radar RASTA (Protat et al. 2009) onboard the French Falcon 20 aircraft. About half of the 20 missions flown by this aircraft, were conducted over southern France allowing gathering information about the physical and radiative properties of ice particles.

Examples of data collected by these various sensorsin a variety of weather situations including a long-lasting bow-echo system (IOP6, 24 Sep 2012), a frontal system associated with embedded convection (IOP8, 29 Sep 2012) and a fast moving isolated thunderstorm (IOP 16, 21 Oct 2012), are presented hereafter.

High-Resolution Observations of Cloud Dynamics and Microphysics

An important asset of HyMeX is the ability to gather observations at the microphysical scale from the TARA and RASTA high-resolution radar profilers. These instruments are both capable of observing the microphysical properties of precipitation at very high spatial and temporal resolutions, i.e. 30m in range every 3s for TARA and 120m every 1.5s for RASTA, and are thus particularly suited to complement stormscale and mesoscale observations provided by scanning weather radars. Both instruments have multi-beam capability.

TARA (Unal et al. 2012) is aS-band (3.298 GHz) ground-based profiling radar with flexible antenna elevation, based on the frequency modulated continuous wave (FMCW) principle. The TARA antenna system include three feeds: a dual-polarized on-focus feed, which is directed along the axis of symmetry of the parabolic reflector (i.e., 45°), and two offset feeds that produce single-polarized beams at 15° angles to the main beam to achieve three dimensional wind speed measurements (additional information about TARA can be found in electronic supplement #2).

An example of TARA capabilities is provided in Fig. 2 using data collected during the IOP8 frontal precipitation event (29 Sep 2012). The time series of observed reflectivity (Fig. 2a), horizontal wind speed (Fig. 2b), and wind direction (Fig. 2c) allow the evolution in precipitation processes to be observed for a 5-hour time period (10-15 UTC),and provide the ability to highlight differences between precipitation and cloud areas during the passage of a frontal system. TARA observations also provide insights into microphysical processes active within clouds, as illustrated by the differential reflectivity (Z_{DR}) spectrogram shown in Fig. 2d. In this figure, Z_{DR}values (related to particle shape) at each height bin are expressed in terms of Doppler velocity, which provides information about the particle fall velocity and, to a further extent, to the particle size and density distribution. From this particular example one can for instance notice (1) an increase of ice particle size in the cloud region (related to the increase of Doppler velocity values), (2) a slight decrease of raindrops size while following towards the ground and (3) a change from spherical to oblate shape of the raindrops as the Doppler velocity (and therefore size) increase.

RASTA is a cloud radar that can be either operated from the ground or from a mobile platform. During HyMeX, it was operated onboard the French Falcon 20 research aircraft (the reader is referred to electronic supplement #3 for more information about this radar). The

airborne version of RASTA has a unique configuration, which consists of six antennas, three looking downward and three looking upward, providing 3D observations of the dynamics and the microphysics of clouds above and below the flight track. Once the cross track, along track and vertical wind fields are retrieved, one can estimate the terminal fall velocity (V_t), which is then combined with radar reflectivity to compute microphysical properties of observed clouds such as ice water content, ice particle density and effective radius (Delanoë et al. 2007). Examples of RASTA observations obtained during IOP 8 are shown in Fig.3.

All in all, TARA can monitor the temporal evolution of cloud processes by observing the same atmospheric column at high temporal resolution, while RASTA can be used to provide accurate spatial distribution of such processes over the a larger area of interest. This complementarity shall be investigated in the near future by using RASTA data collected during the numerous passages of the F20 aircraft over TARA (e.g., Fig. 3e).

Retrieval of Rainfall Drop Size Distributions

The disdrometer network was deployed to monitor the variability of DSD at ground level, as well as to provide relevant information for both polarimetric radar data interpretation and radar rainfall estimation assessment. Collected DSD data can be used to evaluate the performance of radar based DSD retrieval algorithms as well as to establish local power laws adapted to the Cevennes area for the interpretation of radar observations. This potential is illustrated in Fig. 4 which shows the temporal evolution of the rainfall rate, total drop concentration and median volume diameter as observed by disdrometers along the south-north MRR transect (Fig. 1b) and within the Hpiconet area on 29 Sep. 2012 (IOP 8). The large distances between Candillargues,

Alès and the HPiconet area (Fig. 1b) generate a clearly visible time shift in DSD evolution. The small-scale variability of the DSD is illustrated by the range of values measured by the different disdrometers within the Hpiconet network.

Evaluation of Hydrometeor Classification (HID) Algorithms

A major advantage of radar polarimetry is the ability to infer the species of hydrometeors composing precipitating systems. This capability is important to attain many objectives of the HyMeX research program such as the evaluation of new microphysical schemes developed for high-resolution NWP systems, the investigation of relationships between radar observables and variables of interest (e.g., rain intensity), and between cloud microphysics and lightning activity (see below). In this regard, a particular emphasis was put on the evaluation and improvement of hydrometeor classification algorithms at X,-C-, and S-band frequencies.

Figure 5 presents preliminary results of an ongoing study focusing on evaluating the consistency of microphysical retrievals at C- (Montclar radar) and S-band (Nimes radar) by comparing microphysical retrievals within a common sampling area of the two radars. The fuzzy logic algorithm used in this study is based upon the approaches proposed by Al-Sakka et al. (2013), Dolan et al. (2013), Park et al. (2009) and Marzano et al.(2006). It discriminates between six hydrometeor species (rain, wet snow, dry snow, ice, graupel and hail) at S, C and Xband. Overall, the fraction of hydrometeor types inferred from the global analysis of 4 hours of radar data collected during IOP 8 (Fig. 5b) show good consistency despite the different wavelengths and slightly different beam properties of the two radars (1.1° vs. 1.25° beam width).The time

series of hydrometeor species retrieved from the two radars by steps of 5 minutes (Fig 5c-d) are also generally in good agreement although some dissimilarity could be observed around 14 UTC.

In order to better quantify the performance of this, or other, HID algorithms, statistical studies and systematic comparisons with in-situ (FSSP-100, PIP, 2-DS) data will be conducted using flight level data collected during all F20 missions flown over France.Detailed radar intercomparisons will also be reinforced and expanded by taking the research polarimetric X-band radars NO-XP and MXPOL into account in the analysis.

Real-Time 3D Wind Retrieval

The ability to perform multiple-Doppler wind synthesis from operational weather radar systems on a real-time basis was investigated by the French Weather Service in 2006 using a network of six Doppler radars covering the greater Paris area (Bousquet et al. 2007, 2008a). In preparation for the field phase of HyMeX, this analysis was tested over regions of complex terrain of Southern France (Beck and Bousquet, 2013) before being eventually extended to the entire French radar network so as to produce a nationwide, 3D reflectivity and wind field mosaic (Bousquet and Tabary, 2014). During the HyMeX field phase, a special version of this radar mosaic was used to guide the Falcon 20 research aircraft over the Cévennes and Rhone valley areas. Multiple-Doppler wind (MDW) and reflectivity fields were produced in real-time every 15 minutes over a domain of 200 km x 200 km using the six operational radars shown in Fig 1a.

Figure 6 presents examples of real-time, high resolution (1 km^2), multiple Doppler analyses of radar data collected within the bow echo observed during HyMeX IOP6. At the time of

observations, the MCS exhibited many common characteristics of bow-echo systems (Fujita 1978, Davis et al. 2004) such as a strong (24 ms^{-1}), 5-km deep, subsiding rear-to-front (RTF) inflow jet, cyclonic and anti-cyclonic book-end vortices, and strong vertical motion (> 12 m^{-1}) along the leading edge, in addition to strong deep convection with reflectivity values of 25 dBZ up to 12 km amsl. In the near future, these high quality wind fields will be further improved by taking into account research radar data collected during SOP1 into the analysis. In addition to providing insights about the dynamics of MCSs sampled during HyMeX, MDW will also be used to assess (and eventually correct) numerical model forecasts through identifying possible temporal or spatial phase shifts in model outputs (e.g., Beck et al., 2014, Bousquet et al. 2008b).

The HyMeX field campaign also represents a unique opportunity to compare MDW fields with independent measurements such as in-situ or airborne radar data. With this regard, a comparison between MDW and RASTA winds measured during the IOP 6 flight is presented in Fig. 7. Overall, one can notice a good agreement between the two datasets although RASTA-derived winds obviously show more details due to the superior resolution of airborne measurements (Δh = 500m, Δz = 120m) with respect to ground-based observations(Δh = 1000m, Δz = 500m). Such comparisons between MDW and RASTA-derived winds will be performed for all RASTA flights conducted over France so as to evaluate ground-based and airborne wind retrievals over the plain and high terrain.

Synergy Between Radar and Lightning Observations

Observations collected during HyMeX also offer a unique opportunity to investigate the relationships between microphysics, dynamics, electrification and lightning occurrence in storms

that were observed in southern France.Indeed, during SOP1, total lightning activity, including intra-cloud (IC) and Cloud-to-Ground (CG) flashes, and electrical properties of storms were recorded with a Lightning Mapping Array (LMA, Rison et al., 1999) composed of 12 stand-alone stations, several operational Lightning Locating Systems (e.g., EUCLID), and a set of ground-based research instruments (electric field sensors, acoustics sensors, video cameras) deployed throughout the experimental area.

Different types of convection from early to decaying stages were documented over land and over sea with the LMA. An example of concurrent observations within the IOP-6 storm from 0215-0230UTC is shown in Fig. 8. At this time, the lightning activity was distributed more or less along a north-south direction and extended further north outside the LMA network. It was principally located to the west of significant updrafts, as retrieved from radar observations (Figures 8b and 8c). The deepest convective cell was recorded south of the system with lightning observed up to a height of 12 km amsl (Figure 8e). In this thunderstorm, preliminary analysis of the lightning data suggests that the IC/CG ratio was 110:14 for the period 02:25-02:30, where 64% of CG flashes were of negative polarity. For the studied core, electrical discharges were recorded mainly in cloud regions with reflectivity above 20 dBZ.

Another interesting example illustrating the potential of polarimetric radar observations for lightning studies and vice versa was sampled by NOXP on 21 Oct 2012 (Fig. 9). At the time of observations, the radar data indicate an intense cell characterized by significant signal loss in the liquid phase of precipitation at lower elevation angles. Above the melting layer, Z_{DR} presents an interesting positive/negative couplet associated with decreasing differential phase (Φ_{DP}) in the radial direction.This signature is the result of cross-coupling between orthogonally polarized waves when the radar is operating in simultaneous transmission and reception (STAR) mode.

Radial streaks in Z_{DR} and Φ_{DP} at heights of 7 - 10 km have been attributed to ice crystals oriented by electrostatic fields in regions of storm electrification (Ryzhkov and Zrnic 2007; Hubbert et al. 2010). While these depolarization signatures, which can cause bias in Z_{DR}, are usually considered undesirable (Hubbert et al. 2010), they can also be used as an indicator of strong electrification and thus be used as an opportunity to detect charged ice particles in absence of lightning detection sensor.

As it is believed that lightning frequency is proportional to the product of the downward mass flux of graupels and of the upward mass flux of ice crystals (Deierling et al. 2008), statistical analyses of LMA data combined with ice flux and mass budgets inferred from dual-polarimetric radar observations, MDW analyses and exploitation of vertical profile of reflectivity (VPR) polarimetric models (e.g. Kirstetter et al. 2013) will be relied upon to investigate relationships between dynamics, microphysics and lightning activity. These results will also be used to evaluate the explicit lightning scheme CELLS recently implemented in the Meso-NH research model (Barthe et al. 2012, Pinty et al. 2013).

Towards the Assimilation of New Radar Observations

Dual-polarimetric observations

An expected outcome of the HyMeX project is to thoroughly assess the quality of dual-polarimetric radar measurements, as well as to investigate new avenues for their utilization in operational weather forecasts. Specifically, this objective includes the development of data assimilation techniques to ingest dual-polarimetric radar data into convection-permitting NWP

models. A necessary step for data assimilation was the development of a flexible, fully-featured, radar simulator of polarimetric radar variables (e.g., Jung et al. 2008; Pfeifer et al. 2008; Ryzhkov et al. 2011) within the mesoscale, non-hydrostatic, atmospheric model Meso-NH (Lafore et al. 1998) to enable direct comparisons between model-simulated and observed polarimetric radar variables. The newly developed polarimetric radar simulator, which is based on the conventional radar simulator of Caumont et al. (2006), calculates electromagnetic wave propagation and scattering at S, C, and X bands and considers beam propagation effects such as (differential) attenuation and phase shift, and beam refraction and broadening. It is fully consistent with the microphysical parameterizations of the Meso-NH model, which uses a one-moment bulk microphysical scheme governing the equations of the six following water species: vapor, cloud water, liquid water, graupel, snow, and pristine ice. It can be used to simulate all polarimetric observables such as reflectivity at horizontal polarization, Z_{DR}, Φ_{DP}, specific differential phase shift (K_{DP}) as well as cross-correlation coefficient and differential backscattering phase, among others.

An example of observed and simulated polarimetric variables is shown in Fig. 10 for the IOP6 bow echo system. According to observed (Fig. 10a, c, e) and simulated (Fig. 10b, d, f) polarimetric data, the MCS appears reasonably well reproduced by the model although one can note that the convective line is slightly shifted northwestward and that the simulated values are lower than their observed counterparts. These spatio-temporal lags and biases will be considered "innovations" in a data assimilation context, providing needed information to adjust model state variables and improve forecasts at later times. Future work with these datasets will identify the most useful polarimetric observables for data assimilation purposes and will eventually establish

the degree to which their assimilation improves short term forecasts of heavy precipitation events.

Real-time radar refractivity retrieval

Radar refractivity measurements consist in using the signal returned by ground clutter to estimate the refractive index, which is related to surface pressure, temperature, and especially the humidity (Fabry et al. 1997). These observations represent a unique dataset that can be used to map the distribution of low-level moisture, a key parameter for understanding convection initiation and evolution (Besson et al, 2012).

The HyMeX campaign was chosen as a test bed for real-time refractivity retrievals by the French weather service. The refractivity retrieval algorithms of Fabry et al. (1997) and Fabry (2004) were first adapted to the characteristics of French operational radars, which are all equipped with magnetron transmitters (Parent du Châtelet et al., 2012), and then applied to three operational S-band radars (Nîmes, Bollène, and Opoul) located in southern France (Fig. 1a). Refractivity retrievals were evaluated through comparisons with automatic weather stations (Fig. 11) as well as NWP outputs using the observation operator described by Caumont et al. (2013). The good agreement between radar-measured, observed, and model-simulated refractivity, demonstrate the ability to achieve real-time, accurate, low-level refractivity measurements from non coherent weather radars and definitely paves the way for assimilating radar refractivity measurements in convection-permitting NWP models.

Summary and Outlooks

The ongoing deployment of operational and research polarimetric radar systems throughout the planet allow for a whole new world of challenges to the international radar community. With this regard, the radar observations collected in Southern France during HyMeX SOP1 represent a valuable, and potentially unique, dataset that can be used to improve our knowledge of physical processes at play within coastal orographic heavy precipitating systems, but also to develop,and to evaluate, novel radar-based products for research and operational activities. For this reason, radar data collected by international teams involved in the project have all been made freely available on the HyMeX database (http://mistrals.sedoo.fr/HyMeX/) for non-commercial research and educational outreach activities. The use and dissemination of these data and products are encouraged by all radar scientists to foster collaborations and discussions between international research teams from all over the world.

The HyMeX 10-year concerted experimental effort, which has brought together more than 400 scientists from all over the world, will last till 2020 (Drobinski et al. 2014). Although no new field phase is expected at the moment, the HyMeX database will continue to be regularly enhanced with new observations from operational weather services and local field experiments. Collaborations and discussions between scientists will also continue under the auspices of the HyMeX international workshop series, which is being organized every year since 2007.

Acknowledgements:

We wish to thank all the scientists who contributed to the realization of the HyMeX radar component. A special mention is due for the members of Météo-France operational observation

division who managed to provide operational data to the HyMeX community – B. Fradon, H. Al-Sakka, A.-A. Boumahmoud, J. Parent-du-Chatelet and P. Tabary – as well as to scientists – S. Coquillat, M. Hagen, L. Labatut, Y Lemaître, Y. Pointin – and students – E. Fontaine, F. Pantillon, T. Wisman - who participated in field operations and preliminary data analysis. HyMeX SOP1 was supported by CNRS, Météo-France, CNES, IRSTEA, and INRA through the large interdisciplinary international program MISTRALS (Mediterranean Integrated STudies at Regional And Local Scales) dedicated to the understanding of the Mediterranean Basin environmental process (http://www.mistrals-home.org). The radar component of HyMeX SOP1 was sponsored by Grants ANR-2011-BS56-027 FLOODSCALE and ANR-11-BS56-0005 IODA-MED

References

Al-Sakka, H., A.-A.Boumahmoud, B. Fradon, S. Frasier and P. Tabary, 2013: A new fuzzy logic hydrometeor classification scheme for the French X, C and S-band polarimetric radar. *J. Appl. Meteor. Climatol*., in press.

Barthe, C., M. Chong, J.-P.Pinty, C. Bovalo, and J. Escobar, 2012: CELLS v1.0: updated and parallelized version of an electrical scheme to simulate multiple electrified clouds and flashes over large domains, Geosci. Model Dev., **5**, 167-184.

Beck, J. and O. Bousquet, 2013: Using Gap-Filling Radars in Mountainous Regions to Complement a National Radar Network: Improvements in Multiple-Doppler Wind Syntheses. *J. Appl. Meteor. Climatol.*,**52**, 1836–1850.

Beck, J., O. Bousquet and M. Nuret, 2014: Model wind field forecast verification using Multiple-Doppler syntheses from a National Radar Network. *Wea.Forecast.*, in press. doi: http://dx.doi.org/10.1175/WAF-D-13-00068.1

Besson, L., and J. Parent du Châtelet, 2013: Solutions for Improving the Radar Refractivity Measurement by Taking Operational Constraints into Account. *J. Atmos. Oceanic Technol.*, **30**, 1730-1742.

Besson, L., C. Boudjabi, O. Caumont, and J. Parent du Châtelet, 2012: Links between refractivity characteristics and weathers phenomena measured by precipitation radar. *B. Lay. Meteorol.*, **143**, 77-95.

Bougeault, P., P. Binder, A. Buzzi, R. Dirks, R. Houze, J. Kuettner, R. B. Smith, R. Steinacker, and H. Volkert, 2001: The MAP Special Observing Period. *Bull. Amer. Meteorol. Soc.,***82** , 433-462.

Bousquet O. and P. Tabary, 2014: Development of a nationwide real-time 3-d wind and reflectivity radar composite in France. *Q. J. R. Meteorol. Soc.*, in press. doi: 10.1002/qj.2163

Bousquet, O., P. Tabary, and J. Parent du Châtelet, 2008a: Operational multiple-Doppler wind retrieval inferred from long range radar velocity measurements,*J. Appl. Meteor. Climatol.,***47**, 2929–2945.

Bousquet, O., T. Montmerle and P. Tabary, 2008b: Using operationally synthesized multiple-Doppler winds for high resolution NWP model horizontal wind verification. *Geophys. Res. Lett.*, ***35***, L10803, doi:10.1029/2008GL033975.

Bousquet, O., P. Tabary, and J. Parent du Châtelet, 2007: On the value of operationally synthesized multiple-Doppler wind fields, *Geophys. Res. Lett.*, **34**, L22813.

Caumont, O., A. Foray, L. Besson, and J. Parent du Châtelet, 2013: Comparisons between observed and simulated weather radar refractivity change. *B. Lay. Meteorol.*, **148***,* 379–397

Caumont, O., V. Ducrocq, E. Wattrelot, G. Jaubert, S. Pradier-Vabre, 2010 : 1D+3DVar assimilation of radar reflectivity data : A proof of concept. *Tellus*, **62A**, 173–187

Caumont, O., V. Ducrocq, G. Delrieu, M. Gosset, J.-P. Pinty, J. Parent du Châtelet and G. Scialom, 2006 : A radar simulator for high-resolution non-hydrostatic models. *J. Atmos. Ocean. Technol.*, **23**, 1049-1067.

Davis, C., N. Atkins, D. Bartels and co-authors, 2004: The Bow Echo and MCV Experiment (BAMEX): Observations and Opportunities. *Bull. Amer. Meteorol. Soc*., **85**, 1075–1093.

Deierling, W., W. A. Petersen, J. Latham, S. Ellis, and H. J. Christian, 2008: The relationship between lightning activity and ice fluxes in thunderstorms, J. Geophys. Res., 113, D15210, doi:10.1029/2007JD009700.

Delanoë, J., A. Protat, D. Bouniol, A. Heymsfield, A. Bansemer and P. Brown, 2007: The Characterization of Ice Cloud Properties from Doppler Radar Measurements. *J. Appl. Meteor. Climatol.*, **46**, 1682–1698.

Delrieu, G., 2003: L'Observatoire Hydro-meteorologique Mediterraneen Cevennes-Vivarais (The Cevennes-Vivarais Mediterranean Hydro-meteorological Observatory). *La Houille Blanche*, **6**, 83-88.

Delrieu, G., and Coauthors, 2005: The Catastrophic Flash-Flood Event of 8–9 September 2002 in the Gard Region, France: A First Case Study for the Cévennes–Vivarais Mediterranean Hydrometeorological Observatory. *J. Hydrometeor*, **6**, 34–52.

Dolan B., S. A. Rutledge, S. Lim, V. Chandrasekar, M. Thurai, 2013: A Robust C-Band Hydrometeor Identification Algorithm and Application to a Long-Term Polarimetric Radar Dataset. *J. Appl. Meteor. Climatol.*,**52**, 2162–2186.

Drobinski, P. and co-authors, 2014: HyMeX, a 10-year multidisciplinary program on the Mediterranean water cycle. *Bull. Amer. Meteorol. Soc.,*in press. doi: http://dx.doi.org/10.1175/BAMS-D-12-00242.1

Ducrocq, V., and co-authors, 2014: HyMeX-SOP1, the field campaign dedicated to heavy precipitation and flash flooding in the northwestern Mediterranean. *Bull. Amer. Meteorol. Soc.,*in press.doi: http://dx.doi.org/10.1175/BAMS-D-12-00244.1

Dufournet, Y. and Russchenberg, H. W. J., 2011: Towards the improvement of cloud microphysical retrievals using simultaneous Doppler and polarimetric radar measurements, *Atmos. Meas. Tech.*, **4**, 2163-2178.

Fabry, F., 2004: Meteorological value of ground target measurements by radar. *J. Atmos. Oceanic Technol.*, **21**, 560–573.

Fabry, F., C. Frush, I. Zawadzki, and A. Kilambi, 1997: On the extraction of near-surface index of refraction using radar phase measurements from ground targets. *J. Atmos. Oceanic Technol.*, **14**, 979–987.

Fujita, 1978: *Manual of downburst identification for project NIMROD*. Satellite and Mesometeorology Res. Pap.**156**, University of Chicago, Dept. of Geophysical Sciences, pp. 104.

Hubbert, J. C., S. M. Ellis, M. Dixon, G. Meymaris, 2010: Modeling, Error Analysis, and Evaluation of Dual-Polarization Variables Obtained from Simultaneous Horizontal and Vertical Polarization Transmit Radar. Part II: Experimental Data. *J. Atmos. Oceanic Technol.*, **27**, 1599–1607.

Jung, Youngsun, Guifu Zhang, Ming Xue, 2008: Assimilation of Simulated Polarimetric Radar Data for a Convective Storm Using the Ensemble Kalman Filter. Part I: Observation Operators for Reflectivity and Polarimetric Variables. *Mon. Wea. Rev.,***136**, 2228–2245.

Kirstetter, P.-E., H. Andrieu, B. Boudevillain and G. Delrieu, 2013: A Physically Based Identification of Vertical Profiles of Reflectivity from Volume Scan Radar Data. *J. Appl. Meteor. Climatol.*,**52**, 1645–1663.

Kruger A. and W. Krajewski, 2002: Two-dimensional video disdrometer: a description. *J. Atmos. Ocean. Technol.*, **19**, 602-617.

Lafore, J.-P., and Coauthors, 1998: The Meso-NH Atmospheric Simulation System.Part I: adiabatic formulation and control simulations. Scientific objectives and experimental design, *Ann. Geophys.*, **16**, 90-109.

Löffler-Mang, M. and J. Joss, 2000: An Optical Disdrometer for Measuring Size and Velocity of Hydrometeors. *J. Atmos. Oceanic Technol.*, **17**, 130–139.

Löffler-Mang, M., M. Kunz, and W. Schmid, 1999: On the Performance of a Low-Cost K-Band Doppler Radar for Quantitative Rain Measurements. *J. Atmos. Oceanic Technol.*, **16**, 379–387.

Marzano F. S., D. Scaranari, M., P. P. Alberoni, G. Vulpiani and M. Montopoli, 2006: Hydrometeor classification from dual-polarized weather radar: extending fuzzy logic from S-band to C-band data. *Adv. Geosc*., **7**, 109–114.

Medina, S., B. F. Smull, R. A. Houze, Jr., and M. Steiner, 2005: Cross-barrier flow during orographic precipitation events: Results from MAP and IMPROVE. *J. Atmos. Sci.*, **62**, 3580-3598.

Parent du Châtelet, J., C. Boudjabi, L. Besson, and O. Caumont, 2012: Errors caused by long-term drifts of magnetron frequencies for refractivity measurement with a radar: theoretical formulation and initial validation. *J. Atmos. Oceanic Technol.*,**29**, 1428-1434.

Park, H. S., A. V. Ryzhkov, D. S. Zrnić, and K. E. Kim, 2009: The hydrometeor classification algorithm for the polarimetric WSR-88D: description and application to an MCS, *Wea. Forecast.*,**24**, 730–748.

Pfeifer, M., G. Craig, M. Hagen and C. Keil, 2008: A polarimetric radar forward operator for model evaluation. *J. of App.Meteor.*and*Climatol.*,**47**, 3202-3220.

Pinty, J.-P., C. Barthe, E. Defer, E. Richard, and M. Chong, 2013: Explicit simulation of electrified clouds: from idealized to real case studies, *Atmos. Res.*, **123**, 82-92.

Protat, A., and Coauthors, 2009: Assessment of Cloudsat Reflectivity Measurements and Ice Cloud Properties Using Ground-Based and Airborne Cloud Radar Observations. *J. Atmos. Oceanic Technol.*, **26**, 1717–1741.

Rison, W., R.J. Thomas, P.R. Krehbiel, T. Hamlin, and J. Harlin, 1999: A GPS-based Three-Dimensional Lightning Mapping System: Initial Observations in Central New Mexico, *Geophys.* Res. *Lett.*,**26**, 3573-3576.

Rotunno, R. and Houze, R. A., 2007: Lessons on orographic precipitation from the Mesoscale Alpine Programme. *Q.J.R. Meteorol. Soc*., **133**, 811–830.

Ryzhkov, A., M. Pinsky, M., Pokrovsky and A. Khain, 2011: Polarimetric radar observation operator for a cloud model with spectral microphysics. *J. App.Meteor. Climatol.*,**50**, 873-894.

Ryzhkov, A. V. and D. S. Zrnić, 2007: Depolarization in Ice Crystals and Its Effect on Radar Polarimetric Measurements. J. *Atmos. Oceanic Technol*., **24**, 1256–1267.

Schultz, David M., and Coauthors, 2002: Understanding Utah Winter Storms: The Intermountain Precipitation Experiment. *Bull. Amer. Meteor. Soc*., **83**, 189–210.

Stoelinga, Mark T., and Coauthors, 2003: Improvement of Microphysical Parameterization through Observational Verification Experiment. *Bull. Amer. Meteor. Soc.*, **84**, 1807–1826.

Unal, C., 2009: Spectral polarimetric radar clutter suppression to enhance atmospheric echoes .*J. Atmos. Oceanic Technol*., **26**, 1781-1797.

Unal C., Y. Dufournet, T. Otto, and H. Russchenberg, 2012: The new real-time measurement capabilities of the profiling TARA radar. Preprints, *Seventh European Conf. on Radar in Meteorology and Hydrology (ERAD)*, Toulouse, France.

1

List of Figures

Figure 1: Overview of the HyMeX radar network in Southern France during SOP1. (a) Operational radars, (b) Research radars deployed in the Cevennes-Vivarais area (dashed red box in a), (c) Pictures of the main research radars. Color shadings in (a-b) show terrain height. Symbol ^{DP} indicates dual-polarization systems. Symbols S, C and X indicate the radar wavelength.

Figure 2: TARA observations made on 29 Sep. 2012 (IOP 8) over a 5-hour period starting at 1000 UTC. Time series of (a) reflectivity, (b) horizontal wind speed, (c) wind direction, and (d) Z_{DR} spectrogram retrieved at 1055 UTC with negative velocities referring to falling particles. Reflectivity observations allow to monitor the evolution of the precipitation regime (changes in melting layer thickness and vertical rain bands variability), while dynamical information allow to discriminate between air masses (as indicated by black arrows), the transitions being characterized at 0 ms^{-1} horizontal wind speed. In (d) a correction is applied to the Doppler velocity to remove the contribution of the horizontal wind component. Due to heavy turbulence and strong wind shear in the cloud region, this correction artificially produces the zigzag structure seen on the spectrogram.

Figure 3: RASTA measurements and retrieval products made between 13UTC and 16 UTC on 29 Sep. 2012 (IOP8). The vertical reflectivity measured by the nadir and zenith antennas is presented in panel a). Measured radar radial velocities corresponding to vertical, backward and transverse antennas are presented in panels b), c) and d), respectively. Several stack legs at different levels were carried out in the area of Montpellier around Candillargues supersite as shown in panel e). Retrieved zonal and meridional components of the wind are shown in panels f) and g, respectively. Retrieved vertical wind (Vz) and hydrometeors terminal fall velocity (Vt)

are illustrated in h) and i). Ice water content (IWC) is presented in j). The while line in all panels shows the projection of the flight track in the vertical plane. In e) the black star and the green triangle indicate the locations of TARA and Nimes radar, respectively.

Figure 4: Time series of (a) rain rate, (b) total drop concentration and (c) median-volume drop diameter as derived from optical disdrometer measurements at Candillargues (red), Alès (light blue), and all sensors deployed in the Hpiconet (purple) from 10:30-15:50 UTC on 29 September 2012. See Fig. 1 for locations.

Figure 5: (a) Operational reflectivity composite over southern France valid at 1345 UTC, 29 Sep. 2012; (b) Fraction of hydrometeor species retrieved from Nimes (S-band) and Montclar (C-band) radars between 11UTC and 15UTC within a 25 km^2 intercomparison area (red square) shown in (a). Results are shown for (b) the whole period, and by steps of 5 minutes for (c) Nimes and (d) Montclar. In (a) labels Ni and Mo indicate the location of Nimes and Monclar radars, respectively. Within the intercomparison area Mo and Ni radar beams intersect at ~ 3, 7 and 9 km amsl. The two radars are separated from 150 km.

Figure 6: (a) Horizontal cross-section of multiple-Doppler system-relative wind field and reflectivity at 2 km amsl and 0230 UTC on 24 Sep 2012, (b) vertical velocity, and (c) vertical cross-section of reflectivity and multiple-Doppler winds along the red dashed line shown in (a-b). The two insets in (a) show vertical profiles of vertical velocity within the convective area of the system (bottom, star) and zonal wind component within the subsiding RTF inflow area (top, circle), respectively. Dashed black circles in (a) show the location of anticyclonic (bottom) and cyclonic (top) vortices. Gray shadings in (a-b) show terrain height above 500m.

Figure 7: Preliminary comparisons between RASTA-derived (left panel) and Multiple-Doppler (right panel) 3-D winds between 6:30 UTC and 9 UTC, 24 September 2012. a-b) zonal, c-d) meridional and e-f) vertical wind components. Multiple-Doppler data are extracted along the flight track at the closest location of the antenna beam.

Figure 8: (a) reflectivity and horizontal wind at 5 km amsl from 3D Multiple-Doppler wind and reflectivity analysis from 0215-0230 UTC on 24 Sep 2012, (b) overlay of lightning activity as recorded by LMA (in grey along the depth of the 500m reflectivity layer; in white over the entire atmospheric column) and EUCLID (-CG strokes as triangles; +CG strokes as circles) during 15 minutes, (c) vertical velocity, (d) zoom in the domain drawn in (a) with lightning observations collected at 02:29:06-02:29:16 where 7 flashes were recorded by the LMA including one -CG flash in the considered domain, and (e) vertical distribution of the VHF sources overlaid on the vertical cross section of reflectivity along the black line drawn in (d).

Figure 9: (a) Reflectivity, (b) differential reflectivity, and (c) differential phase sampled by NOXP at 1845 UTC on 21 Oct 2012 at an elevation angle of 6.4˚. The red circles highlight depolarization signatures potentially indicating strong electrification in the storm.

Figure 10: Observed (left panel) and simulated (right panel) PPIs of polarimetric variables at an elevation of 0.6° for the Nimes radar, valid on 24 Sept 2012 at 0300 UTC.(a-b) reflectivity (dBZ),(c-d) specific differential phase (° km^{-1}), and (e-f) differential phase (°). Range rings indicate distances of 100 km and 200 km from the radar. White color corresponds to reflectivity value below noise level, while gray color indicates non-meteorological echoes (for radar images) or data outside the domain of simulation (model images*)*.

Figure 11: Time series of radar- (orange), automatic weather station- (AWS, green) and model-

derived refractivity between 10 Aug and 30 Nov 2012, at Nîmes-Garons airport. The blue curve corresponds to 5 minute rainfall rates. The three refractivity maps(bottom) show the evolution of air masses on 24 Sep 2012 at (a) 0700 UTC, (b) 0755 UTC and (c) 0900 UTC. High refractivity values, corresponding to cold and/or wet air masses, are progressively replaced by lower values, which are indicative of warm and/or dry air resulting from the advection of cold air associated with the passage of an eastward propagating cold front over the radar. The black (red) star corresponds to the location of the radar (Nimes-Garons AWS).

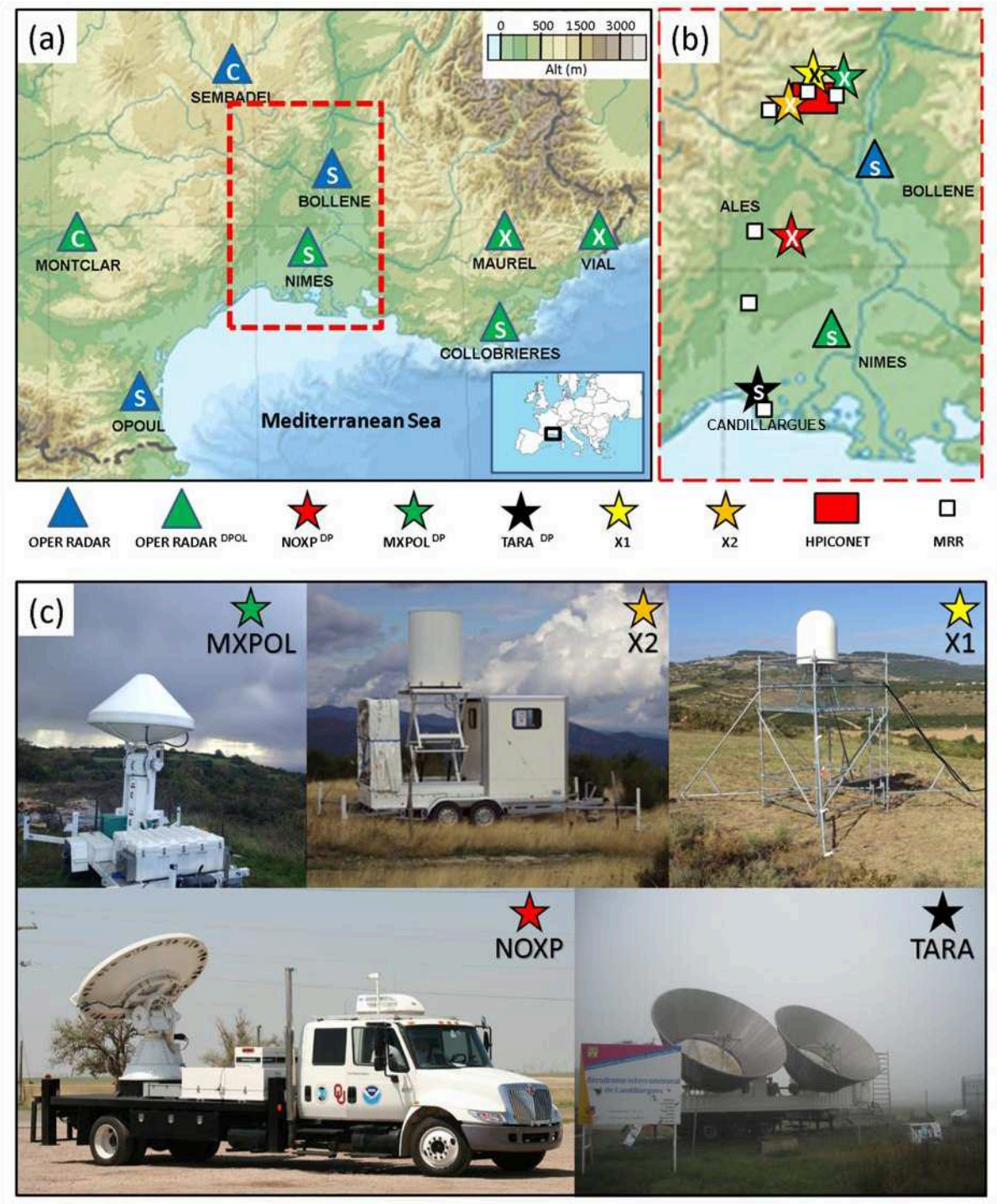

Figure 1: Overview of the HyMeX radar network in Southern France during SOP1. (a) Operational radars, (b) Research radars deployed in the Cevennes-Vivarais area (dashed red box in a), (c) Pictures of the main research radars. Color shadings in (a-b) show terrain height. Symbol ^{DP} indicates dual-polarization systems. Symbols S, C and X indicate the radar wavelength.

1

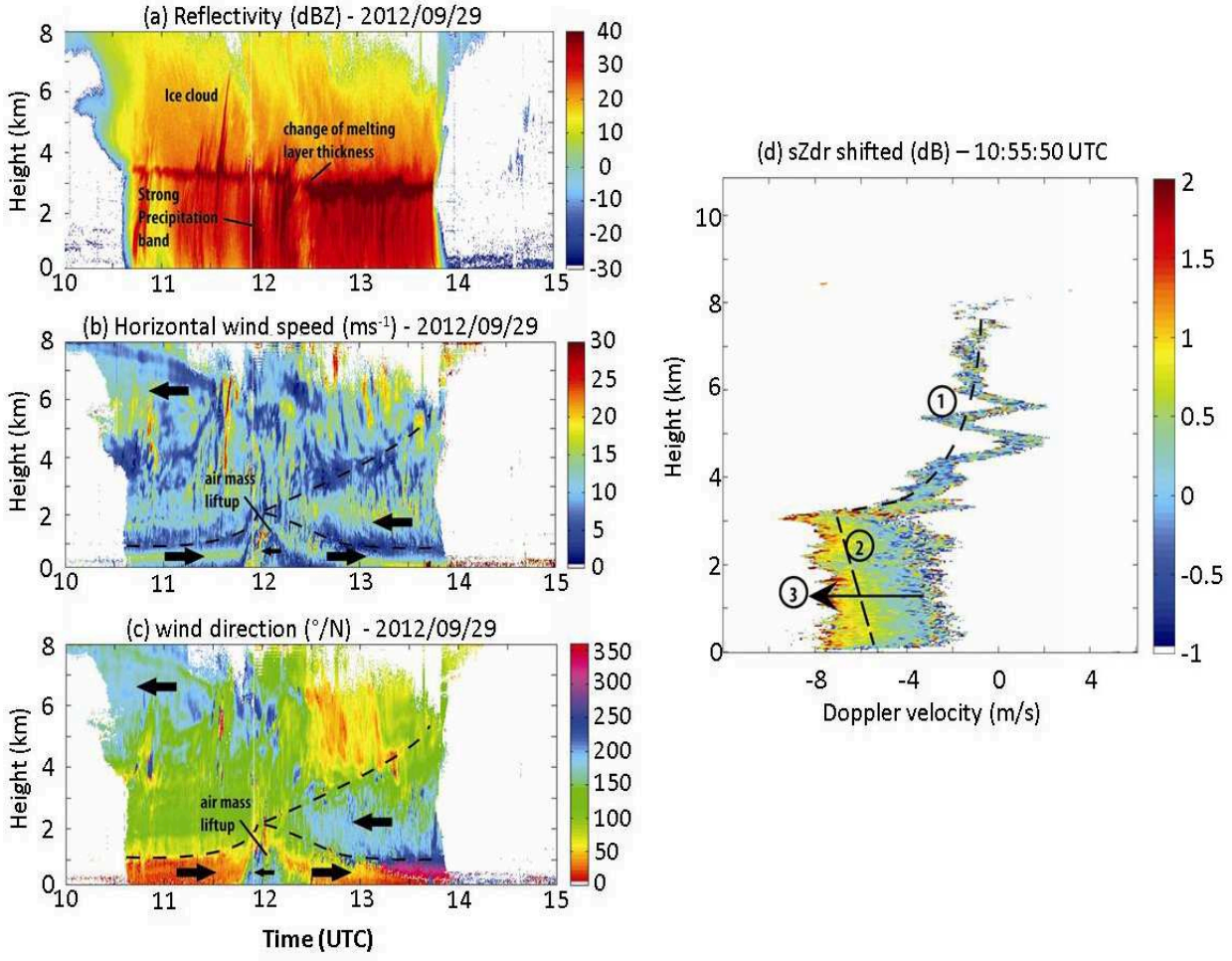

Figure 2: TARA observations made on 29 Sep. 2012 (IOP 8) over a 5-hour period starting at 10UTC. Time series of (a) reflectivity, (b) horizontal wind speed, (c) wind direction, and(d) Z_{DR} spectrogram retrieved at 1055 UTC with negative velocities corresponding to falling particles.Reflectivity observations allow to monitor the evolution of the precipitation regime (changes in melting layer thickness and vertical rain bands variability), while dynamical information allow to discriminate between air masses (as indicated by black arrows), the transitions being characterized at 0 ms^{-1} horizontal wind speed. In (d) a correction is applied to the Doppler velocity to remove the contribution of the horizontal wind component. Due to heavy turbulence and strong wind shear in the cloud region, this correction artificially producesthezigzagstructure seenon the spectrogram.

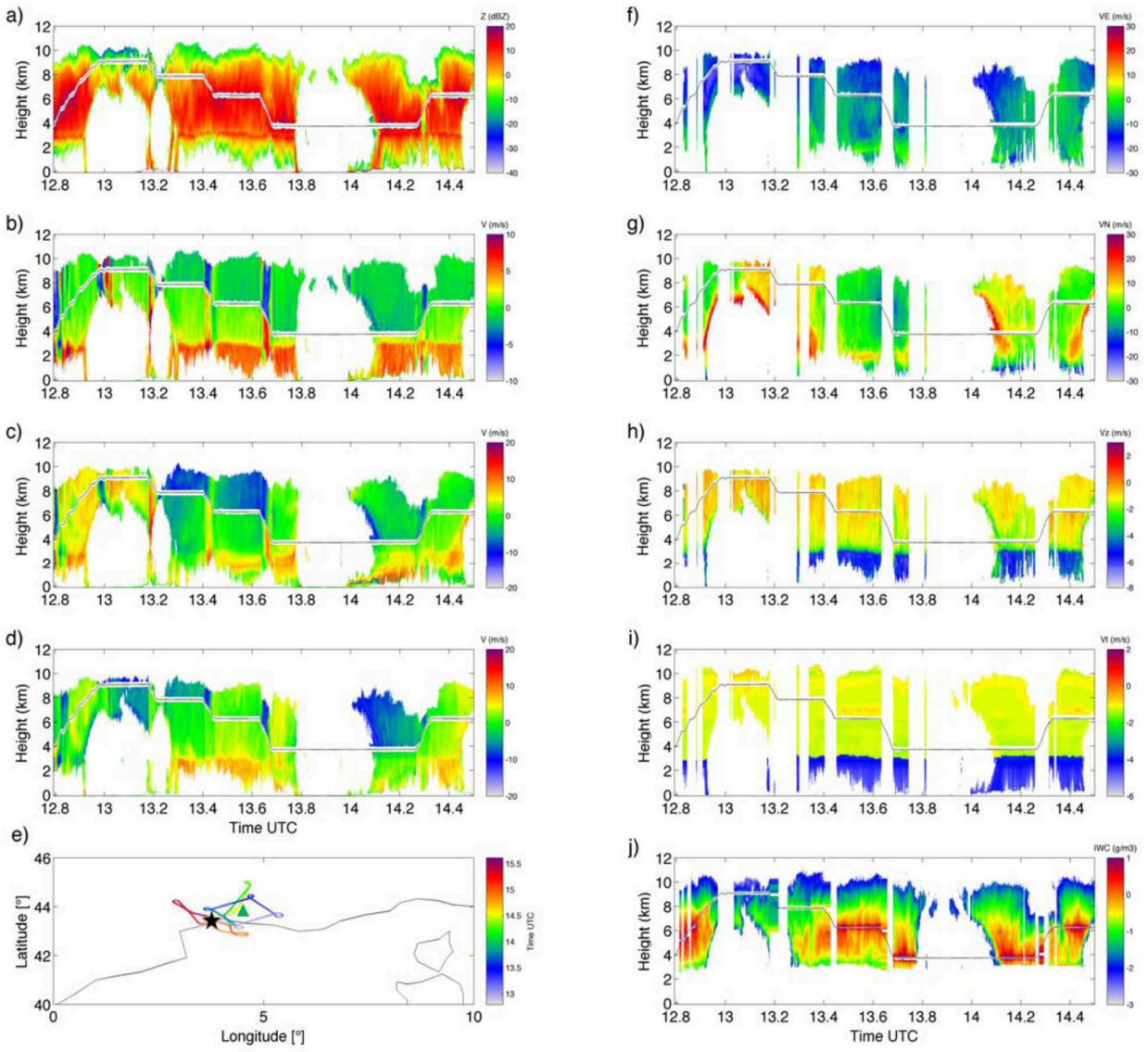

Figure 3: RASTA measurements and retrieval products made between 13 and 16 UTC on 29 Sep. 2012 (IOP8). The vertical reflectivity measured by the nadir and zenith antennas is presented in panel a). Measured radar radial velocities corresponding to vertical, backward and transverse antennas are presented in panels b), c) and d), respectively. Several stack legs at different levels were carried out in the area of Montpellier around Candillargues super site as shown in panel e). Retrieved zonal and meridional components of the wind are shown in panels f) and g, respectively. Retrieved vertical wind (Vz) and hydrometeors terminal fall velocity (Vt) are illustrated in h) and i). Ice water content (IWC) is presented in j). The while linein all panels shows the projection of the flight track in the vertical plane. In e) the black star and the green triangle indicate the locations of TARA and Nimes radar, respectively.

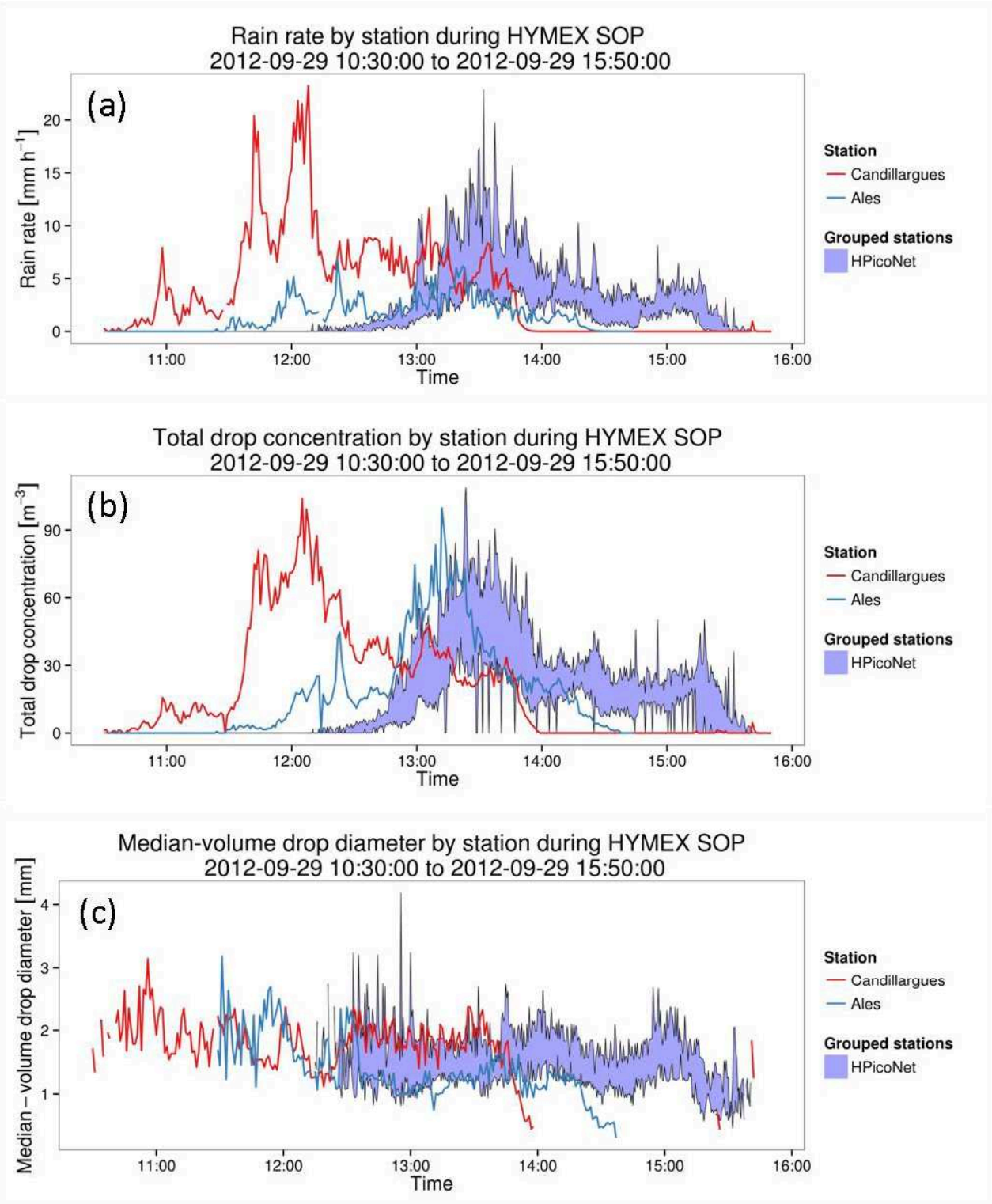

Figure 4: Time series of (a) rain rate, (b) total drop concentration and (c) median-volume drop diameter as derived from optical disdrometer measurements at Candillargues (red), Alès (light blue), and all sensors deployed in the Hpiconet (purple) from 10:30-15:50 UTC on 29 September 2012. See Fig. 1 for locations.

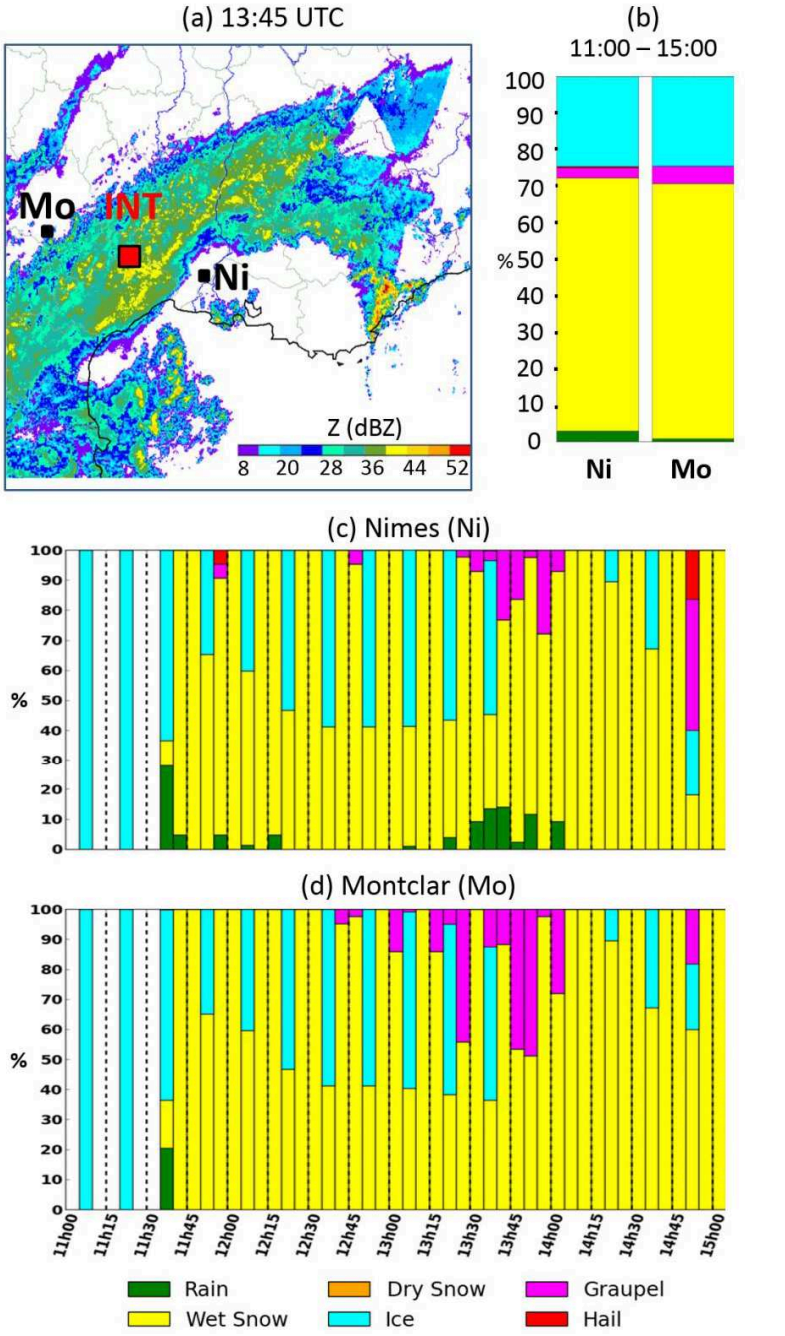

Figure 5: (a) Operational reflectivity composite over southern France valid at 1345 UTC, 29 Sep. 2012; (b) Fraction of hydrometeor species retrieved from Nimes (S-band) and Montclar (C-band) radars between 11UTC and 15UTC within a 25 km^2 intercomparison area (red square) shown in (a). Results are shown for (b) the whole period, and by steps of 5 minutes for (c) Nimes and (d) Montclar. In (a) labels Ni and Mo indicate the location of Nimes and Monclar radars, respectively. Within the intercomparison area Mo and Ni radar beams intersect at ~ 3, 7 and 9 km amsl. The two radars are separated from 150 km.

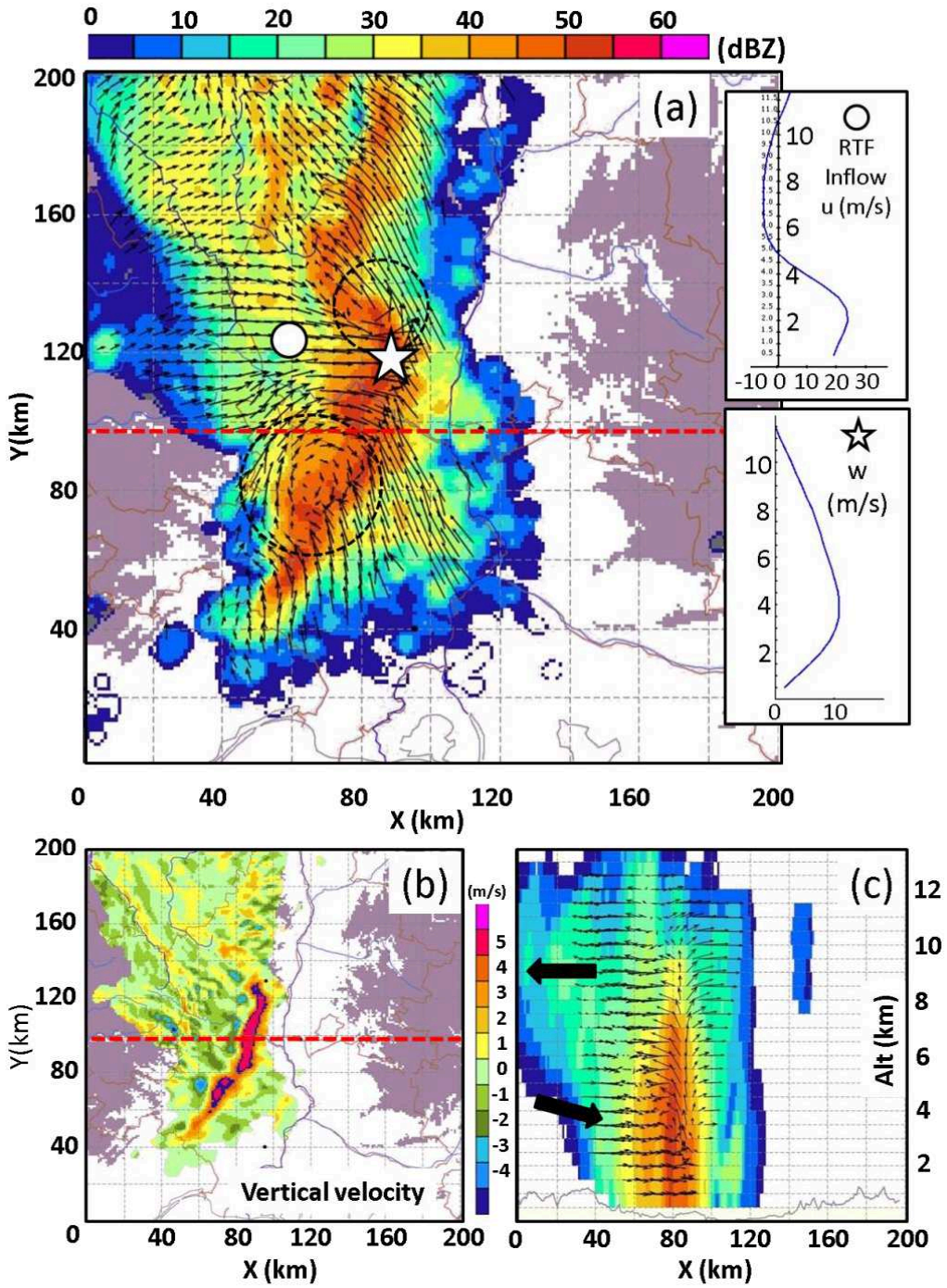

Figure 6: (a) Horizontal cross-section of multiple-Doppler system-relative wind field and reflectivity at 2 km AMSLand 0230 UTC on 24 Sep 2012, (b) vertical velocity, and (c) vertical cross-section of reflectivity and multiple-Doppler winds along the red dashed line shown in (a-b). The two insets in (a) show vertical profiles of vertical velocity within the convective area of the system (bottom, star) and zonal wind component within the subsiding RTF inflow area (top, circle), respectively. Dashed black circles in (a) show the location of anticyclonic (bottom) and cyclonic (top) vortices. Gray shadings in (a-b) show terrain height above 500m.

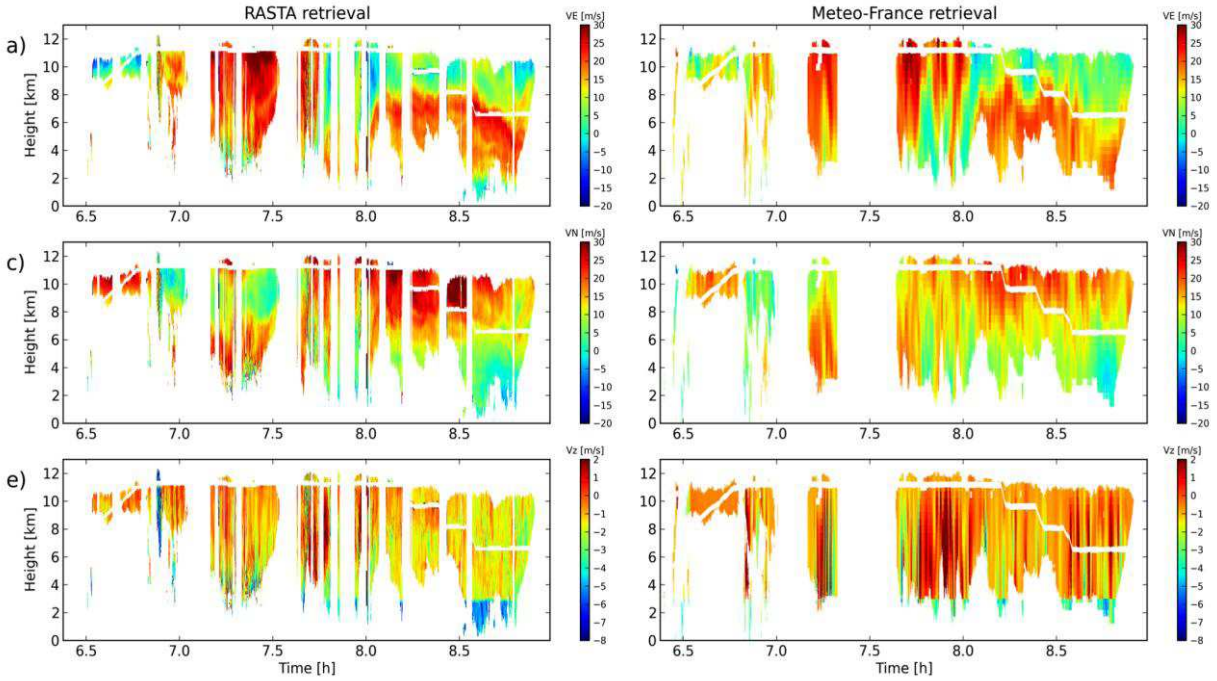

Figure 7: Preliminary comparisons between RASTA-derived (left panel) and Multiple-Doppler (right panel) 3-D winds between 6:30 UTC and 9 UTC, 24 September 2012. a-b) zonal, c-d) meridional and e-f) vertical wind components. Multiple-Doppler data are extracted along the flight track at the closest location of the antenna beam.

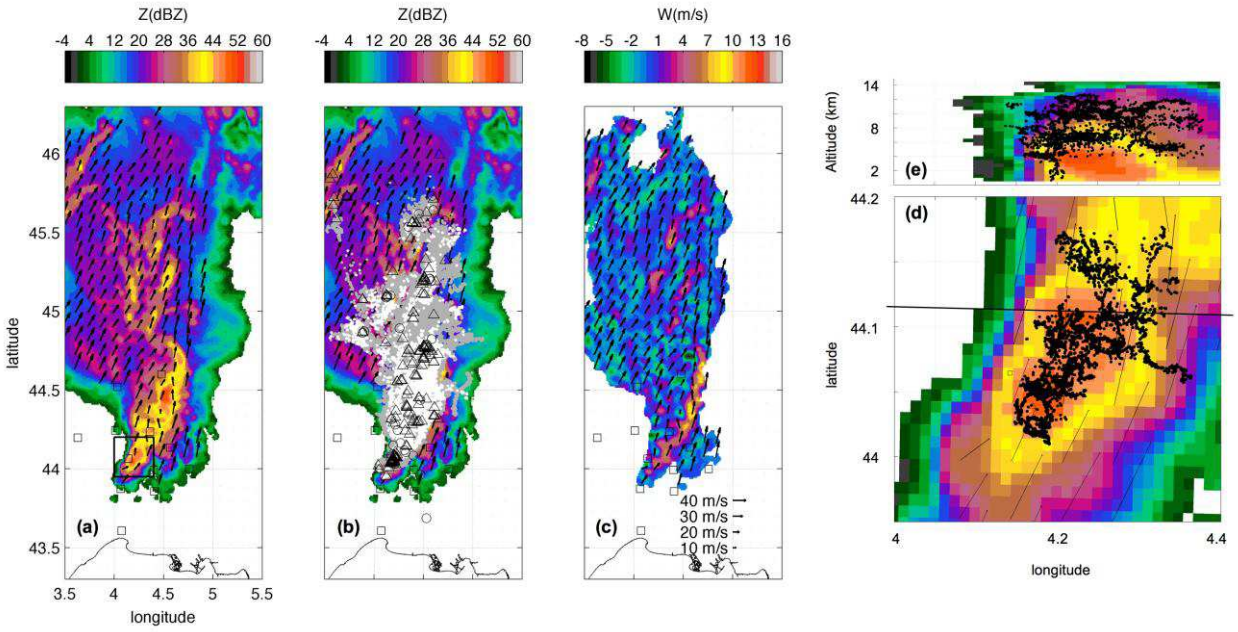

Figure 8: (a) reflectivity and horizontal wind at 5 km amsl from 3D Multiple-Doppler wind and reflectivity analysis from 0215-0230 UTC on 24 Sep 2012, (b) overlay of lightning activity as recorded by LMA (in grey along the depth of the 500m reflectivity layer; in white over the entire atmospheric column) and EUCLID (-CG strokes as triangles; +CG strokes as circles) during 15 minutes, (c) vertical velocity, (d) zoom in the domain drawn in (a) with lightning observations collected at 02:29:06-02:29:16 where 7 flashes were recorded by the LMA including one -CG flash in the considered domain, and (e) vertical distribution of the VHF sources overlaid on the vertical cross section of reflectivity along the black line drawn in (d).

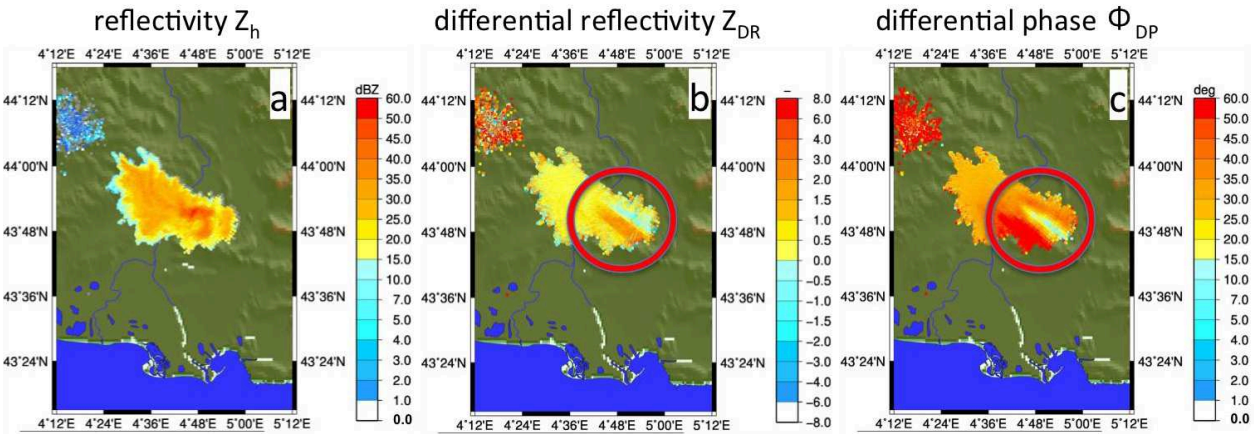

Figure 9: (a) Reflectivity, (b) differential reflectivity, and (c) differential phase sampled by NOXP at 1845 UTC on 21 Oct 2012 at an elevation angle of 6.4˚. The red circles highlight depolarization signatures potentially indicating strong electrification in the storm.

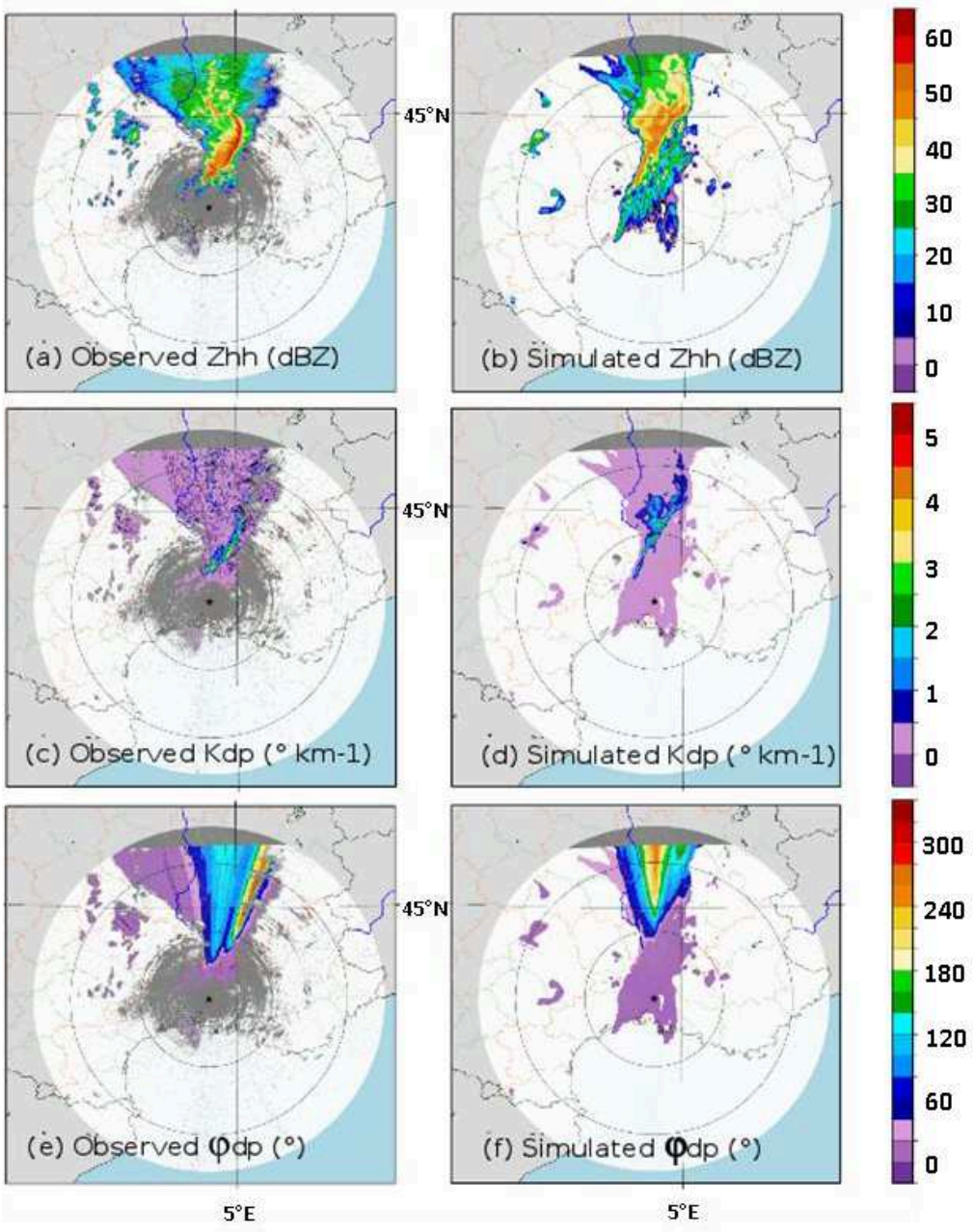

Figure 10: Observed (left panel) and simulated (right panel) PPIs of polarimetric variables at an elevation of 0.6° for the Nimes radar (see Fig. 1 for location), valid on 24 Sept 2012 at 03 UTC.(a-b) reflectivity (dBZ), (c-d) specific differential phase (° km^{-1}), and (e-f) differential phase (°).Range rings indicatedistances of 100 km and 200 km from the radar. White color corresponds to reflectivity value below noise level, while gray color indicates non-meteorological echoes (for radar images) or data outside the domain of simulation (model images).

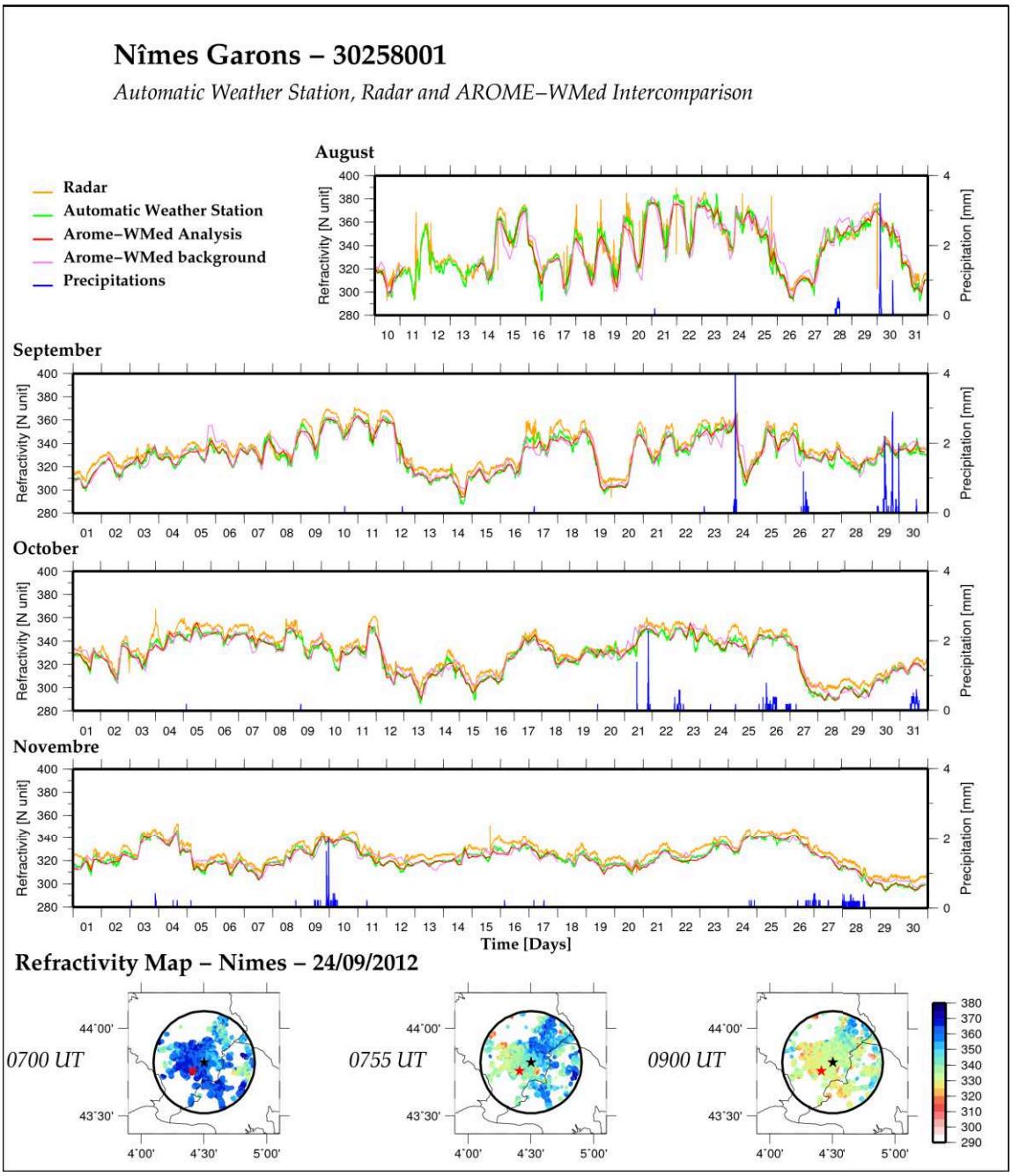

Figure 11: Time series of radar- (orange), automatic weather station- (AWS, green) and model-derived refractivity between 10 Aug and 30 Nov2012, at Nîmes-Garons airport. The blue curve corresponds to 5 minute rainfall rates. The three refractivity maps(bottom) show the evolution of air masses on 24 Sep 2012 at (a) 0700 UTC, (b) 0755 UTC and (c) 0900 UTC. High refractivity values, corresponding to a cold and/or wet airmasses, are progressively replaced by lower values, which are indicative of warm and/or dry air resulting from the advection of cold air associated with the passage of an eastward propagating cold front over the radar. The black (red) star corresponds to the location of the radar (Nimes-Garons AWS).

ELECTRONIC SUPPLEMENTS

ES #1 **Instrument location and main specifications**

LOCATION	Type	Latitude (°N)	Longitude (°E)	Altitude (m)	Owner
RESEARCH RADARS					
Candillargues (TARA)	S Dpol	43,61	4,06	2	TU Delft
La Bombine (X1)	X	44,51	4,03	1020	LaMP
Le Chade (X2)	X	44,58	4,47	268	LaMP
Montbrun (MXPOL)	X Dpol	44,61	4,54	330	EPFL
Mount Bouquet (NOXP)	X Dpol	44,13	4,28	620	NSSL
OPERATIONAL RADARS*					
Bollène	S	44,32	4,75	309	MF
Collobrières	S Dpol	43,21	6,36	640	MF
Montclar	C Dpol	44,01	2,6	667	MF
Mont Maurel	X Dpol	44,01	6,53	1773	MF
Mont Vial	X Dpol	43,89	7,15	1525	CNRS
Nimes	S Dpol	43,81	4,5	71	MF
Opoul	S	42,92	2,85	704	MF
Sembadel	C	45,28	3,7	1115	MF
MICRO RAIN RADARS					
Alès	MRR	44,13	4,09	150	NASA
Banne	MRR	44,36	4,15	310	DLR
Candillargues	MRR	43,61	4,06	2	MF
Pradel-Grainage	MRR	44,57	4,50	270	LaMP
Saint-Etienne-de-Fontbellon	MRR	44,60	4,38	210	LTHE
Saint-Mélany	MRR	44,52	4,12	300	LaMP
DISDROMETERS					
Alès	2DVD	44,13	4,09	150	NASA
Alès	OD	44,13	4,09	150	LTHE
Banne	OD	44,36	4,15	310	DLR
Blaches	OD	44,6	4,48	440	EPFL
Candillargues	OD	43,61	4,06	2	UB
La Souche	OD	44,62	4,12	920	LTHE
Lavilledieu	OD	44,57	4,45	230	EPFL
Lussas	OD	44,61	4,47	290	EPFL
Mirabel-Mairie	OD	44,6	4,4986	500	EPFL
Mont-Redon	OD	44,61	4,51	630	LTHE
Nîmes-Courbessac	OD	43,85	4,4	60	NASA
Pradel-Ferme	OD	44,58	4,4985	270	EPFL
Pradel-Ferme-bis	OD	44,58	4,4985	270	EPFL

Pradel-Grainage	2DVD	44,57	4,5	270	EPFL
Pradel-Vignes	OD	44,58	4,495	270	LTHE
Quissac	OD	43,9	4,01	80	EPFL
Saint-Etienne-de-Fontbellon	OD	44,6	4,38	210	LaMP
Saint-Germain-Ecole	OD	44,55	4,44	200	EPFL
St-Jean-du-Gard	OD	44,09	3,88	250	NASA
Saint-Mélany	OD	44,52	4,12	300	LaMP
Saint-Quentin-la-Poterie	OD	44,04	4,44	110	NASA
Tourgueille	OD	44,12	3,66	540	LTHE
Uzès	OD	43,99	4,4	70	NASA
Valescure	OD	44,09	3,83	480	LTHE
Villeneuve-de-Berg	OD	44,55	4,4953	300	LTHE
Villeneuve-de-Berg-2	OD	44,55	4,4953	300	LTHE
Villeneuve-de-Berg-3	OD	44,55	4,4954	300	LTHE

Acronyms

Dpol : Dual-polarimetric ; **OD** : Optical disdrometer ; **2DVD**: 2-D Video disdrometer

CNRS: Centre National de la Recherche Scientifique, France
DLR : DeutschesZentrumfürLuft- undRaumfahrt, Germany
EPFL: Ecole Polytechnique Fédérale de Lausanne, Switzerland
LaMP : Laboratoire de Météorologie Physique, France
LTHE : Laboratoire d'étude des Transferts en Hydrologie et Environnement, France
MF : Météo-France, France
NASA: National Aeronautics and Space Administration, USA
NSSL : National Severe' Storm Laboratory, USA
TU-Delft: Delft University of Technology, The Netherlands
UB: University of Barcelona, Spain

* The reader is referred to Bousquet and Tabary (2014, QJRMS) for more information about operational radar systems.

ES #2 TARA characteristics

Frequency (GHz)	3.298
Vertical resolution (m)	3-75 m
Range (km)	15
Integration time (s)	2.56
Peak power (W)	Non applicable (FMCW)
Nyquist velocity (m s^{-1})	7.5
Antenna size (m)	3 (2.1° beam width)
Sensitivity at 1km (dBZ)	-20

1

2

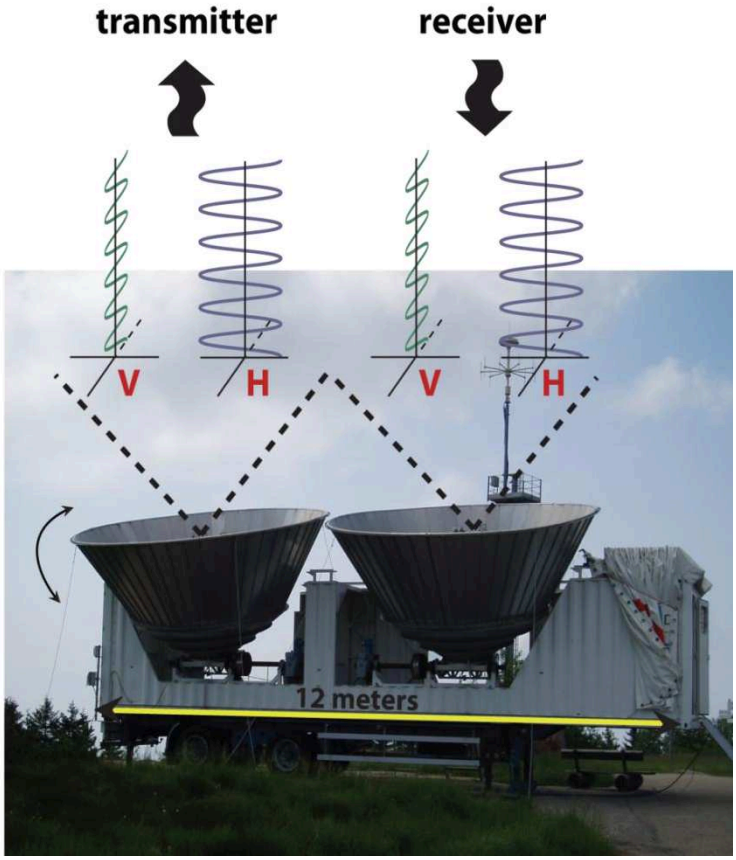

3

ES #3 RASTA characteristics

Frequency (GHz)	95.04
Vertical resolution (m)	60
Horizontal resolution (m)	225 to 300 depending on aircraft speed
Range (km)	15
Integration time (ms)	250 (measurement every 1.5 s for each antenna)
Peak power(kW)	2
Nyquist velocity (m s^{-1})	8
Antenna size (cm)	30 to 60 (0.35°/0.7° beam width)
Sensitivity at 1km (dBZ)	-32 to -16 depending on considered antenna
FALCON speed (m s^{-1})	150-200
angles of the tilted antennas	Nadir, 38° off-nadir in the direction of propagation of the aircraft, and 20° off-nadir perpendicular to the direction of propagation of the aircraft.
Calibration	Bouniol et al. 2008 *J. Atmos. OceanicTechnol., 25, 1983–1995.*

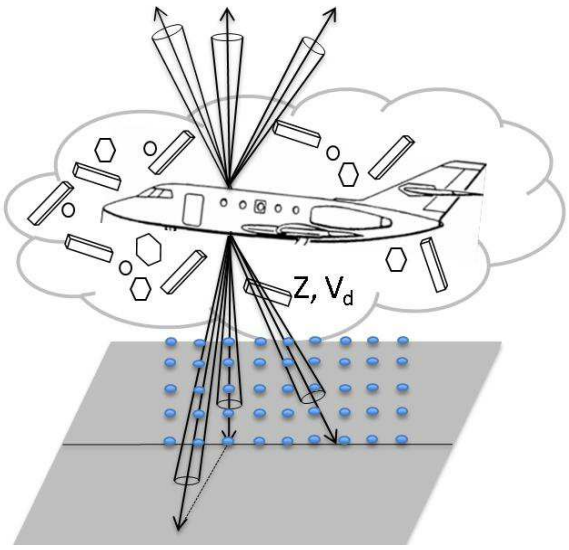

RASTA sampling strategy and antenna configuration

Supplemental Material

Click here to download Supplemental Material: BAMS_radar_revised_ES.docx